

Received July 24, 2021, accepted July 29, 2021, date of publication August 3, 2021, date of current version August 11, 2021.

Digital Object Identifier 10.1109/ACCESS.2021.3102190

Potential Visible-Light Driven PtO₂/GaN vdW Hetero-Bilayer Photocatalysts for Water Splitting Using First-Principles

MD. SAKIB HASAN KHAN¹, MUHAMMAD SHAFFATUL ISLAM²,
MD. RAFIQU L ISLAM¹, (Senior Member, IEEE), AHMED ISKANDERANI³,
IBRAHIM M. MEHEDI^{3,4}, (Member, IEEE),
AND MD. TANVIR HASAN⁵, (Senior Member, IEEE)

¹Department of Electrical and Electronic Engineering (EEE), Khulna University of Engineering & Technology (KUET), Khulna 9203, Bangladesh

²Department of Electrical and Electronic Engineering (EEE), World University of Bangladesh (WUB), Dhaka 1205, Bangladesh

³Department of Electrical and Computer Engineering (ECE), King Abdulaziz University, Jeddah 21589, Saudi Arabia

⁴Center of Excellence in Intelligent Engineering Systems (CEIES), King Abdulaziz University, Jeddah 21589, Saudi Arabia

⁵Department of Electrical and Electronic Engineering (EEE), Jashore University of Science and Technology (JUST), Jashore 7408, Bangladesh

Corresponding author: Md. Tanvir Hasan (tan_vir_bd@yahoo.com)

This work was supported by the Deanship of Scientific Research (DSR), King Abdulaziz University, Jeddah, under Grant DF 755-135-1441.

ABSTRACT Novel two-dimensional (2D) PtO₂/GaN van der Waals (vdW) hetero-bilayers (HBL) are studied here for photocatalytic water splitting (PWS) application under first-principles density functional theory (DFT). We proposed six HBLs due to the atomic orientational variations and two of them are found dynamically stable confirmed by phonon dispersion curves. The two stable HBLs, HBL1, and HBL6 also show negative binding energy depicted by the interlayer distance-dependent binding energy curves. Among them, HBL1 has the lowest binding energy, suggesting the exothermic practicability of the material. Electronically both materials show a visible ranged indirect bandgap of ~ 2.65 (2.69) eV for HBL 1 (HBL6), lowered by ~ 2 times compared to their intrinsic constituents (2D PtO₂, 2D GaN). The bandgaps also have type-II band orientation, which is highly required for efficient spatial carrier separation in photocatalytic water splitting (PWS) applications. The optical properties of the HBLs were also calculated, and it's found that the HBLs have $\sim 2 \times 10^5 \text{ cm}^{-1}$ of perovskite material-like absorption coefficient in the visible spectrum, a key requirement for efficient photocatalysis. Reflectivity is as low as $\sim 7\%$ in the visible spectrum, suggesting the low-loss nature of the materials. Photocatalytic band-edges with type-II band alignments show sufficient kinetic overpotential for hydrogen evolution reaction (HER) and oxygen evolution reaction (OER) in both HBLs, suggesting effective water-splitting capacity. Moreover, we have explored the biaxial strain-induced tunability of the electronic bandgap, absorption coefficients, and photocatalytic band edges. They all found responsive due to homogeneous biaxial strain and show bandgap-lowering, absorption coefficient visible shifting, and band-edges tuning from compressive to tensile strains in the -6% to $+6\%$ range. These studies suggest that the novel PtO₂/GaN vdW layered material can be a probable efficient material for visible-light-driven photocatalytic water-splitting technology.

INDEX TERMS 2D PtO₂/GaN, hetero-bilayer, van der Waals (vdW) concept, first-principles density functional theory (DFT), optoelectronic property, photocatalytic water splitting.

I. INTRODUCTION

The incremental energy consumption is made globally, causing a detrimental environmental effect as the energy sources

The associate editor coordinating the review of this manuscript and approving it for publication was Guijun Li¹.

are mainly from fossil fuels [1]. This leads to CO₂ emission worldwide to the extent that was never before, resulting in serious global warming [2], [3]. An energy alternative, potentially high-efficient, renewable, and facilitated by low- or zero CO₂ -emission is highly demanding to reduce this negative effect. This leads to an eloquently simple concept of hydrogen

TABLE 1. 2D GaN and PtO₂ based vdW structures in literature as photocatalysts.

Materials	E _g (eV)	Remarks	Ref.
ZnO/GaN	2.82-D	Type-II, tunability absent	[34], [35]
GaN/GeC	3.47 (MGGA), D	Type-II, tunability present	[15]
GaN/MoSe ₂	1.65-1.7(HSE06), I	Type-II, tunability present	[31]
GaN/WSe ₂	1.7-1.8 (HSE06), D	Type-II, tunability present(slight)	[31]
GaN/BAs	1.7(HSE06), D	Type-II, tunability absent	[28]
MoS ₂ /GaN	1.5 (HSE06), D	Type-II, tunability absent	[29]
BP/GaN	1.6 (HSE06), D, I	Type-II, tunability present	[36]
PtO ₂ /MoS ₂	1.5 (HSE06), I	Type-II, tunability absent	[20]

D = direct bandgap, I = indirect bandgap

(H₂) fuel production from water using a semiconductor-based splitting mechanism [4], [5]. The core attractiveness of the concept is that harnessing the two-dimensional (2D) semiconductor and layered materials-based photocatalysts, the water can be split into oxygen (O₂) and H₂ with zero CO₂-emission while the traditional biomass-gasification process of H₂ fuel production comes up with CO₂ byproduct [6]. However, finding an efficient photocatalyst is on the search, and many scientists are exploring newer and newer possibilities. In this regard, the key challenge is to seek a material having all the attributes for photocatalytic water splitting (PWS). The attributes are the following: the material must possess (i) suitable bandgap (~1.23 eV) and band-edges so that the kinetic overpotential become sufficient for hydrolysis, (ii) spatial carrier separation capability and high-surface to volume ratio so that photocatalytic sites can be increased, and (iii) high-optical absorption in the visible or near ultra-violet (NUV) spectrum so that the peak solar irradiations can be utilized. To acquire these features, nanostructured 2D materials are the best candidates as they have suitable band-gap, high-surface to volume ratio, superior carrier mobility, and considerable absorption co-efficient [5], [7]–[9]. The prominent proof regarding it is the first nanostructured (nanoparticle) photocatalysts, TiO₂ outperforms in water splitting with better hydrogen yield than its bulk structure [7], [10]. From these evidences, many 2D materials are coming into the light for PWS application. Among them, a nonmetallic graphene-like C₃N₄ shows ~3.2 μmol/h/g of H₂ production at ~λ > 420 nm visible lights with ~10 m²/g surface area and ~2.7 eV near-ultraviolet (NUV) bandgap [9], [11]. It shows almost by ~35 (~106 μmol/h/g) times more yields when Pt co-catalysts are added. Bandgap engineered graphene outperforms in this respect almost by ~100 (~1050 μmol/h/g) times more yields than the previous one [5]. Besides, 2D transition metal dichalcogenides (TMDs) show a tangible change (~26000, ~62000, and ~2580 μmol/h/g of yields for MoS₂, MoSe₂, and WS₂, correspondingly) in H₂ yields using their self-polarizing properties [5], [12], [13]. However, the spatial carrier separation, another key requirement for PWS cannot be acquired by only 2D materials. Here, comes another alluring concept, vdW stacked layered materials, as with

the properties like 2D materials, they also have bandgap tunability due to stacking patterns, spatial carrier separation capability, and superior optical absorption [14], [15]. With the advent of nanotechnology, emergent materials, precisely, graphene, 2D oxides, 2D transition metals dichalcogenides (TMDs), and 2D group III-V are experimentally realized and unleashed the astonishingly unique properties of the materials [12], [16], [17]. As such material is 2D PtO₂, having superior thermo-mechanical stability with ~175.78 N/m of mechanical stiffness, two valley bandgap of ~1.67 eV (PBE), ~3.15 eV (HSE06), and ~3.59 eV (GW), superior optical absorption and carrier mobility, is numerously used as substrate material for many-layered materials, hetero-bilayers for photovoltaics and PWS applications [18]. For example, ZnO/PtO₂ vdW hetero-bilayer (HBL), with direct type-II 0.47 eV of bandgap, can be used in photodetector application [19], PtO₂/MoS₂ vdW HBL with indirect bandgap shows photocatalysis property [20], experimentally synthesized Ni(OH)₂/PtO₂ nanostructured array show enhanced hydrogen evolution reaction (HER) [21], and PtO₂ based nanoparticle show improved HER [22]. Besides, the PtO₂ based 2D and vdW structures show altering bandgap, enhanced HER, and improved optical absorption. Another promising 2D material, 2D planar GaN with a large ultraviolet (UV) ranged bandgap ~4.42 eV (GW), and ~4.18 eV-5.2 eV (experimental) bandgap, high thermal and chemical stability, mechanically robustness (~108.37 mechanical stiffness and 0.410 Poisson's ratio), self-polarizing capability, and ultra-high carrier mobility makes it available in wide ranges of application namely, photovoltaics, coating material, UV-detector, and dielectric material for nano-transistors [23]–[26]. It is also experimentally realized [24], [27]. Moreover, the vdW concept of 2D GaN is widely used as direct-Z scheme type-II bandgap photocatalysts for water splitting [15], [28]–[30]. Some of the shreds of evidence are compiled in **TABLE 1**. Among them, 2D GaN stacked with TMDs, and transition metal oxides (TMO) outperforms due to their visible driven PWS capability with cross-plane spatial carrier separation (SCS). Besides, MoS₂/GaN, phosphorene/GaN, GeC/GaN, BAs/GaN, and BP/GaN are all show tunable electronic, optical properties

with tunable PWS band edges due to stacking variations and external perturbation (biaxial strain, and cross-plane electric field) [29], [31]–[33].

However, to our best knowledge, the vdW PtO₂/GaN hetero-bilayer is not studied yet for the PWS application, though 2D PtO₂ and 2D GaN possess astounding intrinsic and tunable optoelectronic properties. Therefore, in this study, we have introduced the novel vdW PtO₂/GaN hetero-bilayer with all of its stacking variants and explore the PWS attributes of the materials. Also, to unlock tunability in electronic, optical, and photocatalytic properties, biaxial strain is introduced. These studies suggest that the novel vdW PtO₂/GaN hetero-bilayer, with visible ranged bandgap, high-optical absorption, and tunable photocatalytic properties can be a promising material for advanced PWS technology.

II. COMPUTATIONAL METHODOLOGY

For the density functional theory (DFT) calculations, **C**Ambridge **S**erial **T**otal **E**nergy **P**ackage (CASTEP), an academic opensource version, is used which utilizes a plane-wave basis set [37]. Electron-ion interactions are described by the norm-conserving pseudopotential (NCP). To predict electronic properties, we initially implemented Perdew-Burke-Erzerhof (PBE) functional with generalized gradient approximation (GGA) exchange-correlation [38]. Conventionally, GGA-PBE exchange-correlation functional predict bandgap underestimated from experimental bandgap of a semiconductor. Heyd-Scuseria-Ernzerhof's (HSE 06) nonlocal hybrid functional was introduced to minimize the bandgap problem [39]. Besides, customized meta-GGA (MGGA) functional with 2D PRHG and regularized PBE is utilized to further reduce the deviation between theoretical and experimental bandgap [40]. We have also evaluated the predicted bandgap value with experimental and quasi-particle (QP) bandgap values. The vdW interaction, significant in the stacked HBLs, is defined by semi-empirical Grimme dispersion corrected density functional theory (DFT-D3) [41]. To model the vdW stacked HBLs, a 2 × 2 supercell of 2D PtO₂ and 2D GaN are chosen and oriented in six different ways. For each 2D layer, a 30 Å vacuum slab model is used.

For structural relaxation Broyden-Fletcher-Goldfarb-Shanno (BFGS) algorithm is used with energy cut-off 800 eV. The energy, stress, force, and displacement tolerance cutoff are 1 × 10⁻⁵ eV/atom, 0.05 GPa, 0.03 eV/Å, and 0.001 Å, correspondingly. The K- points sampling for reciprocal space are 9 × 9 × 1, 15 × 15 × 1, and 30 × 30 × 1 for electronic band structure, projected density of states (PDOS), and optical properties calculations, respectively. For predicting the exothermic feasibility of the stacking, the binding energy is introduced equated by the following equation,

$$E_b = \left[E_{heterobilayer} - \sum_i E_i (layer_i) \right] \quad (1)$$

where, $E_{heterobilayer}$ is the dispersion corrected total energy of the hetero-bilayer system, and $\sum_i E_i (layer_i)$ is the sum of the energies of i numbers of 2D layers for stacking the

hetero-bilayer. Likewise, the formula used for charge density difference calculation is the following,

$$\Delta\rho = \rho_{heterobilayer} - \sum_i \rho_i (layer) \quad (2)$$

here, $\rho_{heterobilayer}$ is the vdW HBL's charge density and $\sum_i \rho_i (layer)$ is the accumulated charge density of the 2D layer used for vdW stacking. Besides, to predict the dynamical stability of the HBLs, density functional perturbation theory (DFPT) initiated phonon dispersion curves are introduced.

For strain-dependent tunability of the properties, the following equation is applied,

$$a_s = \pm e \times a_u + a_u \quad (3)$$

where, a_s and a_u denotes strained and unstrained lattice constants, correspondingly. The e with +ve (-ve) sign signifies the tensile (compressive) strains.

For calculating density functional theory (DFT) based dielectric function, $\varepsilon(\omega) = \varepsilon_1(\omega) + i\varepsilon_2(\omega)$, the complex dielectric constant is evaluated first. Interestingly, a singularity between inter-band transition energies and complex dielectric function is found evaluated by [42], [43],

$$\varepsilon_2 = \frac{2e^2\pi}{\Omega\varepsilon_0} \sum_{k,v,c} |\langle \Psi_k^c | \hat{u} \times r | \Psi_k^v \rangle|^2 \delta(E_k^c - E_k^v - E) \quad (4)$$

where, e = electronic charge, \hat{u} = vector defining the polarization of incident field, Ω = polarization density, r = spatial position, ψ_k^c and ψ_k^v = the conduction band (CB) and valence band (VB) wave-function at k respectively. E_k^c = the conduction band energy, E_k^v = valence band energy, and E = Fermi energy.

III. RESULTS AND DISCUSSION

A. STRUCTURAL PROPERTIES

We have first included here the structural details of our proposed PtO₂/GaN vdW HBLs along with the constituents. The 2D GaN (α -PtO₂) is planar (buckling) with a hexagonal structure (P-3M1). The calculated lattice parameters for 2D α -PtO₂ (GaN) are the following: lattice constant, $a \sim 3.168$ (3.248) Å, bond length, $d_B \sim 2.07$ (1.875) Å, and buckling height, $d_H \sim 1.865$ (0.0) Å. These lattice parameters are well-aligned with other theoretical and experimental studies [18], [26], [31], [42], [44]–[47]. For stacking the 2D layers, 2D PtO₂(α -phase) is assumed as substrate layer and 2D GaN is vertically placed on top of that layer. While stacking, lattice mismatch arises due to the lattice constant discrepancy of the 2D layers and the mismatch is ~ 2.5 %, quite lower compared with other vdW stacked HBLs, as calculated by % mismatch = 100 ($a_{2D GaN} - a_{2D PtO2}$)/ $a_{2D PtO2}$ [15], [19], [28], [34]. This mismatch value is also in the allowable value (below 5%) of the vdW stacking, suggesting the possibility of stacking. The six variants of the HBLs are oriented in the following manner: First, we defined two oxygen atoms in the buckling structure of PtO₂ as upper oxygen (O_u) and lower oxygen (O_l). Now, in HBL 1, gallium (Ga) and

nitrogen (N) atoms stacked on top of platinum (Pt) and O₁ atoms, respectively; in HBL 2, N (Ga) atoms are right on the Pt (O₁) atoms; In HBL 3, Ga atoms are stacked on the Pt atoms and N atoms are on the top of O_u; In HBL 4, N (Ga) atoms are stacked on top of Pt (O_u) atoms; In HBL 5, Ga (N) atoms are directly on top of O₁(O_u) atoms; finally, in HBL 6, the order is reversed i.e., N (Ga) atoms are straight on top of O₁(O_u) atoms. The geometry relaxed structures of the HBLs (HBL 1, and HBL 6) are shown in **Fig 1 (a), and (b)**. **Figure 2** shows the phonon dispersion curves for 2D GaN **(a)**, 2D PtO₂ **(b)**, HBL 1 **(c)**, HBL 2 **(d)**, HBL 3 **(e)**, HBL 4 **(f)**, HBL 5 **(g)**, and HBL 6 **(h)**, including the interlayer binding energy curves **(i)**. The dynamic stability test is done on the HBLs through density functional perturbation theory (DFPT) and the HBL 1 **(Fig.2 (a))**, and HBL 6 **(Fig.2 (h))** are found dynamically stable. The other HBLs, HBL 2, HBL3, HBL4, HBL 5 are dynamically unstable as negative phonon branches are found in the phonon dispersion curves as depicted in **Figs. 2(d - g)**.

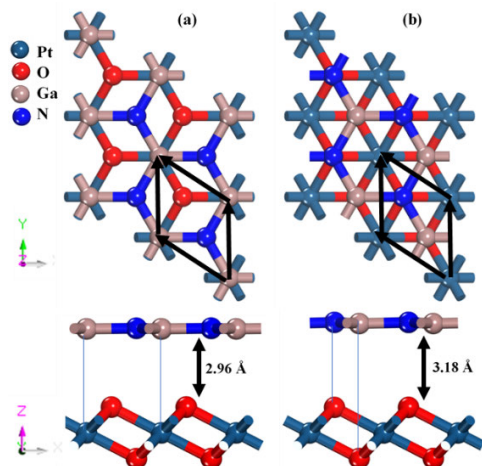


FIGURE 1. VdW stacked models for **(a)** HBL1, and **(b)** HBL6. The black solid lines are for the unit cell of the hetero-bilayer (HBL).

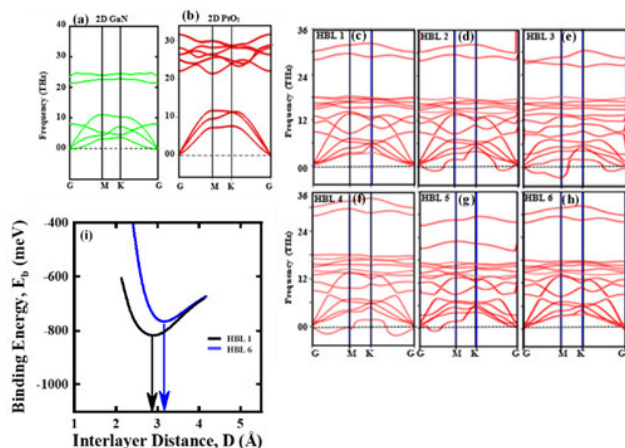


FIGURE 2. Phonon dispersion curves for **(a)** 2D GaN, **(b)** 2D PtO₂, **(c)** HBL 1, **(d)** HBL 2, **(e)** HBL 3, **(f)** HBL 4, **(g)** HBL 5, and **(h)** HBL 6, and **(i)** interlayer binding energy curves.

We have also excluded the unstable HBLs from our further studies. The dynamically stable optimized HBLs have lattice constants ~ 3.209 Å (~ 3.208) Å for HBL 1 (HBL 6), which also remains in the lattice constant range of 2D GaN and 2D PtO₂, as expected as in the theory. Among the HBLs, HBL 1 (HBL 6) has the smallest (highest) interlayer spacing ~ 2.963 Å (~ 3.180 Å).

To reveal the exothermic feasibility of the HBLs, the inter-layer spacing dependent binding energy is calculated by the following equation,

$$E_b = E_{PtO_2/GaN \text{ HBL}} - E_{GaN} - E_{PtO_2} \quad (5)$$

where, $E_{PtO_2/GaN \text{ HBL}}$ = dispersion corrected total energy of the HBL, E_{GaN} = the energy of 2D GaN and E_{PtO_2} = the total energy of 2D PtO₂. The binding energy curves are shown in **Fig.2 (i)**. The binding energies, respective interlayer distances, optimized lattice constants, and buckling heights, bond lengths are enlisted in **TABLE 2**. The binding energy predicts the most energetically favorable HBL and HBL 1 is the most favorable. As strong binding energy means strong interlayer coupling in the HBLs, the HBL 1 has the smallest interlayer spacing with the highest cross-layer coupling. These cross-layer spacing variations appear due to the atomic orientation while stacking. Now, to evaluate whether the HBLs are vdW bonded or covalent bonded, we have calculated the sum of vdW and covalent radii of the stacked atoms. The smallest cross-layer spacing is ~ 2.963 Å in HBL 1, higher than the accumulation of covalent radii of Ga (1.26 Å) and Pt (1.3 Å) atom i.e., 2.56 Å, indicating the absence of covalent bonding between the 2D layers. However, the cross-layer distance is within the accumulated vdW radii of Ga (1.87 Å) and Pt (1.75 Å) atom i.e., 3.62 Å, referring to the existence of vdW interaction in between the stacked layers.

B. ELECTRONIC PROPERTIES OF HETERO-BILAYER SYSTEM

To implement our user-defined meta-GGA (MGGA) for the rest of the electronic properties, we have evaluated the functional by comparing with experimental value and quasiparticle (QP) GW bandgap value. The comparison of GGA-PBE, HSE 06, GW, and experimental bandgap with customized MGGA (2D PRHG with 2D corrected PBE) is depicted along with the band structures in **Fig. 3 (a)-(h), (i)**. The bandgap values we have calculated using various functionals are in correspondence with the other theoretical and experimental studies. The wonder is that the customized MGGA well-predicts the bandgap with acceptable accuracy as compared with the GW bandgap ($\sim 5\%$ deviation from GW in 2D GaN) and experimental (our proposed MGGA underestimates 2D GaN bandgap ~ 0.82 eV while GW approximation underestimates the bandgap ~ 1.04 eV). These comparisons suggest that the customized MGGA is well-suited for almost $\sim 90\%$ reducing of computational cost within acceptable accuracy (e.g., GW requires 64 CPU hours while MGGA requires only 2 CPU hours for the same type of calculations). The

TABLE 2. Optimized lattice constant a (Å), bond length d_B (Å), buckling Height, d_H (Å), cross-layer binding energy, E_b (meV), cross-layer spacing, D (Å), bandgap E_g^{PBE} (eV) using GGA-PBE functional, bandgap E_g^{HSE06} (eV) using HSE-06 non-local functional, and bandgap E_g^{MGGA} (eV) using Meta-GGA (MGGA) functional with 2D PRHG.

Structure	a (Å)	d_B (Å)	d_H (Å)	E_b (meV)	D (Å)	E_g^{PBE} (eV)	E_g^{HSE06} (eV)	E_g^{MGGA} (eV)
2D GaN	3.248	1.875	0.0	-	-	2.29 K/G	3.42 K/G	4.291 K/G
2D PtO ₂	3.168	2.07	1.865	-	-	1.90 G/M*	3.57 G/M*	4.847 G/M*
HBL 1	3.209	-	-	-820	2.963	0.42 K /M*	1.04 K /M*	2.650 K /M*
HBL 6	3.208	-	-	-770	3.180	0.49 K /M*	1.08 K /M*	2.690 K /M*

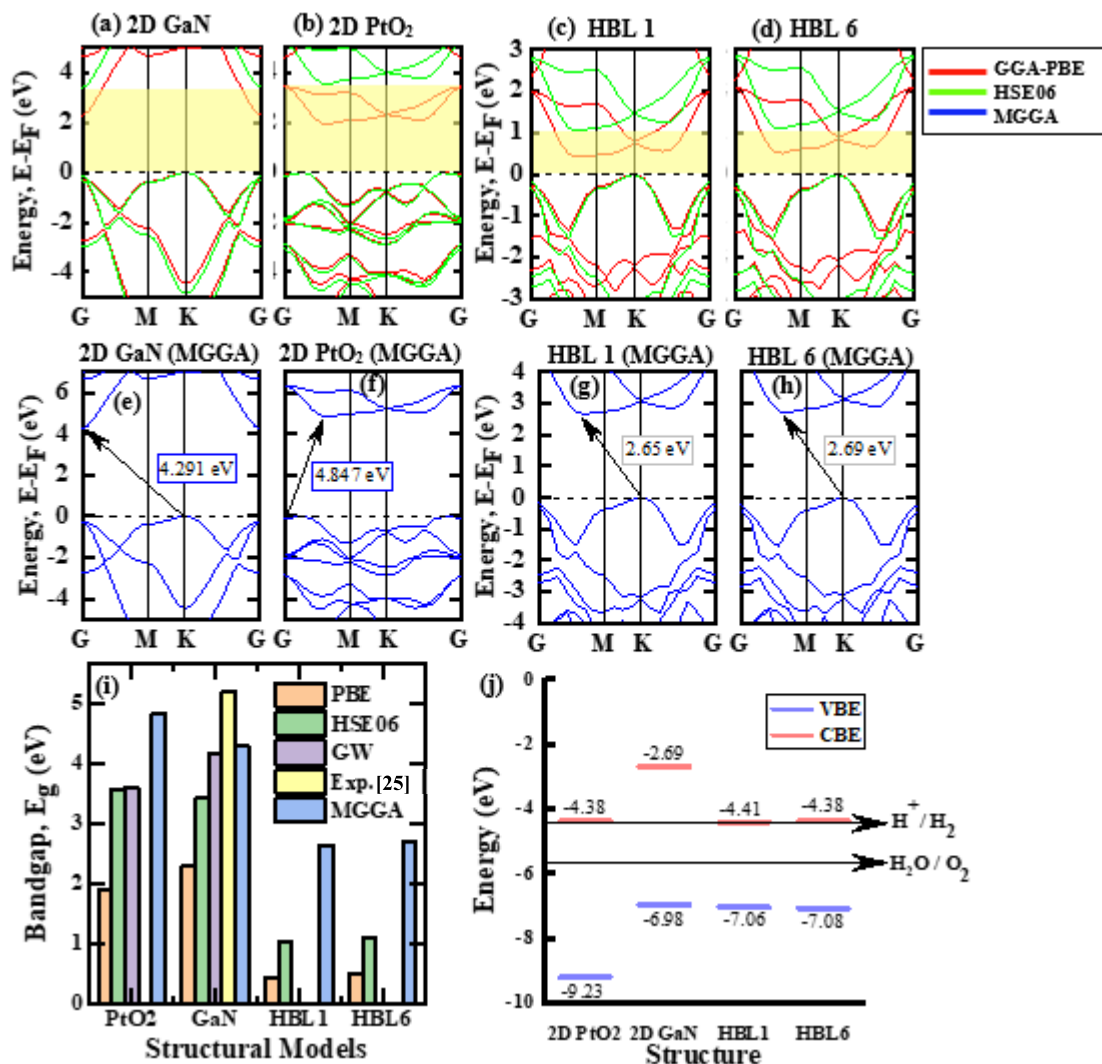


FIGURE 3. The band-structures calculated by GGA-PBE, and HSE06 for (a) 2D GaN, (b) 2D PtO₂, (c) HBL 1, (d) HBL 6. The band structures calculated by customized MGGA functional for (e) 2D GaN, (f) 2D PtO₂, (g) HBL 1, (h) HBL 6. (i) Comparative bandgap values. (j) Relative band alignment for 2D GaN, 2D PtO₂, HBL1, and HBL6 for photocatalytic water splitting.

MGGA band structures of the HBLs are also depicted in Fig. 3 (e)-(h). As depicted, the bandgap values are highly receptive in the value due to stacking. The HBL 1 and HBL 6 both have indirect bandgap with almost ~2 times lowering of the bandgap values from their constituents, facilitating for the PWS application.

To evaluate the photocatalytic water splitting activity of the VdW HBL, the relative band edges are to be calculated. For this purpose, the MGGA bandgap values are considered utilizing the equation $E_{CB} = X - E_e - (\frac{E_g^{MGGA}}{2})$ for conduction band edge (CBE) and $E_{VB} = X - E_e + (\frac{E_g^{MGGA}}{2})$ for valance

band edge (VBE) calculation. Where, the Mulliken electronegativities of the comprising atoms of the hetero-bilayers are denoted by X , E_e represents the standard hydrogen potential (4.45 eV). The Mulliken electronegativity for 2D GaN (PtO₂) is 4.83 eV (6.80 eV). **Fig 3 (j)** demonstrates the VBE and CBE for the 2D GaN, 2D PtO₂, HBL 1, and HBL 6. The relative band-edge positions suggest that VBE is contributed by 2D GaN, and CBE contributed by 2D PtO₂, outlining the type-II band edge (staggering). At, pH level zero, the standard potential with respect to vacuum for (2H⁺/H₂) reduction and (H₂O/O₂) oxidation potentials are at -4.46 eV, and -5.67 eV energy levels, respectively. In comparison with these reference values, both HBL 1 and HBL 6 have adequate kinetic overpotential for initiating the reduction and oxidation (redox) reactions, facilitating the hydrolysis potentiality. Moreover, the valance band offset (VBO) (conduction band offset (CBO)) is ~ 2.25 eV (1.69 eV), high enough to separate the carrier spatially. This high-VBO and CBO thus facilitates the potentiality of the photocatalysis of the water.

For the deep insights, we have evaluated the atomic orbital projected density of states (PDOS) (as shown in **Fig. 4 (a), and (b)**) so that the band-edge contributing atoms and their orbitals can be revealed. In both HBLs, the CBE is mainly subsidized by the d-orbital of Pt atom of the 2D PtO₂ layer, and the VBE is dominantly donated by p-orbital of N atom of the 2D GaN layer, marking the type-II (staggering) band positions. This finding is also theoretically in line with the relative band-edge calculation mentioned in the previous paragraph.

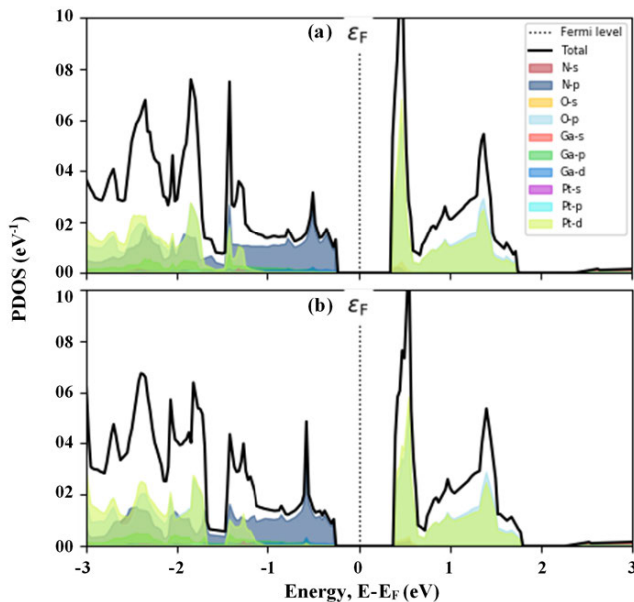


FIGURE 4. Atomic orbital projected density of states (PDOS) (GGA-PBE) for (a) HBL 1, and (b) HBL 6.

To gain the insights of charge transfer and contributing layers, the charge density difference is shown using, $\Delta\rho = \rho_{HBLs} - \rho_{2DPtO_2} - \rho_{2DGaN}$, where, ρ_{HBLs} is the charge density of HBL, ρ_{2DPtO_2} is the charge density of 2D PtO₂

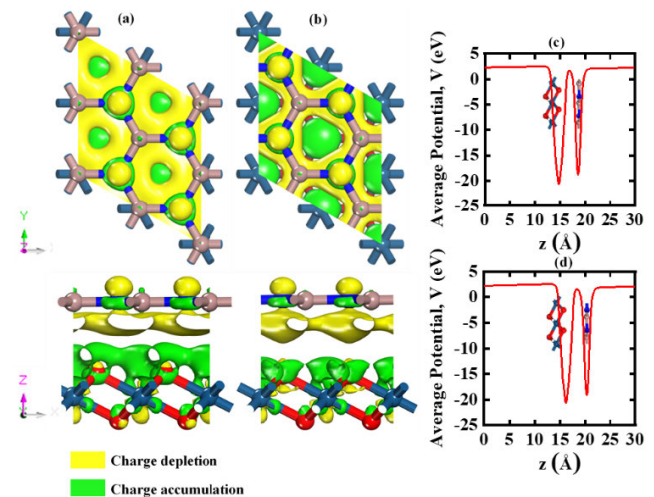


FIGURE 5. The charge density differences plot for (a) HBL 1, and (b) HBL 6. The yellow (green) color represents the charge depletion (accumulation). The iso value is assumed ~ 0.001 e Å⁻³. Effective average potential differences for (c) HBL 1, and (d) HBL 6 are shown by red solid lines concerning the z-axis.

and P_{2DGaN} is the charge density of the 2D GaN. The yellow (green) region refers to the charge depletion (accumulation). In both HBL (**Fig 5. (a), (b)**), N (O) predominantly depletes (accumulates) the charges. This nature signifies the charge transfer direction from N atoms of 2D GaN to O atoms of 2D PtO₂. The transfer is also confirmed by the comparative electro-negativities of the atom. As, the O atoms (~ 3.44) have higher electro-negativity than N atoms (~ 3.04), resulting in the charge transfer from N to O direction.

To find out the effective carrier separation capability, the spatial effective average potential along the cross-plane direction is calculated from the Poisson equation. It turns out that 2D PtO₂ has a higher potential than 2D GaN which is reliable with the charge transmission as well. A significant amount of effective potential difference ~ 3.25 V is found. A strong electrostatic electric field arises due to the high-potential difference which results in spatially discretizing the charge carriers, operating as anti-recombinant, highly suggestive for photocatalysis applications. To proceed further, we have calculated the electron and hole effective masses of the HBLs and comprising 2D layer from dispersion band theory as summarized in **TABLE 3**. The values reveal that the electron and hole effective masses are highly responsive to the stacking orientation of the HBLs. However, the HBLs

TABLE 3. Calculated effective mass m_e^*/m_0 .

Structure	m_e^*/m_0	m_h^*/m_0
2D GaN	0.467	1.018
2D PtO ₂	0.902	1.782
HBL 1	0.844	1.612
HBL 6	0.782	1.335

show a low value of effective masses compared with their constituents, suggesting high-carrier mobility in the HBLs. Moreover, effective carrier separation is also suggestive due to the low recombination time as mobility is higher, also confirming the potential of spatial carrier separation and facilitating the PWS.

C. ELECTRONIC PROPERTIES OF HBLs: BIAxIAL STRAIN CONTRIBUTION

Biaxial strain, an intrinsic feature of vdW stacked HBL, arisen from the lattice mismatch is used here to alter the electronic properties. The biaxial strain tuned band structures for HBL 1 and HBL 6 are shown in Fig. 6 (a), (b). Unstrained HBL 1 shows an indirect bandgap ~2.65 eV

at K (VBM) to M* (CBM). With increasing the compressive strains, the bands at the K point become lower and at the gamma (G) point pushed up, resulting in the bandgap increment from ~2.65 eV to 2.82 eV at 4% compressive strain. Simultaneously, the conduction band minima (CBM) are shifted toward the G point and pushed down due to the application of compressive strains. This trends also lower the bandgap value at 6% compressive strain and the bandgap becomes ~2.71 while at 4% compressive strain it is ~2.82 eV. Tensile strains, on the other hand, push up the band near the K point in the VBM and shift the band in the CBM from M* to M, resulting in the bandgap lowering with the increase of tensile strains. As a whole, both compressive and tensile strains seem to lower the bandgap value. In HBL 6, a similar fashion is observed with compressive and tensile strains. However, the highest bandgap is attained ~2.87 eV at 4% compressive strain.

To evaluate the band edge tunability due to the biaxial strain, we have calculated the CBE and VBE upon applying biaxial strains as depicted in Fig 7 (a), (b). It is found that

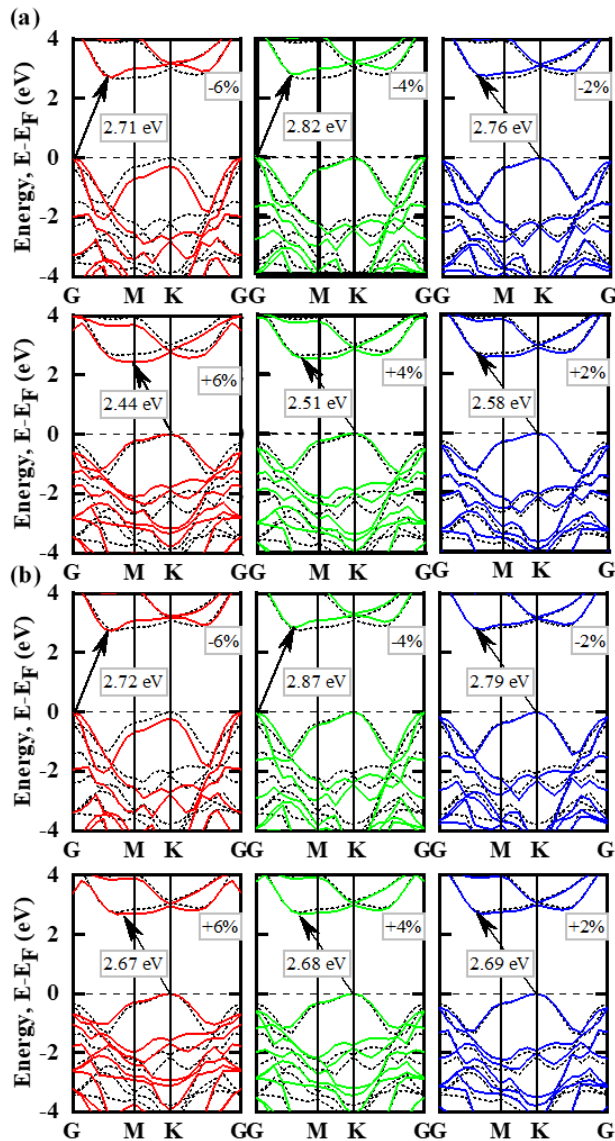


FIGURE 6. Biaxial strain-tuned band structures upon 6% compressive to 6% tensile strain range for (a) HBL 1, and (b) HBL 6. Dotted lines show unstrained bands and solid lines represent strained bands.

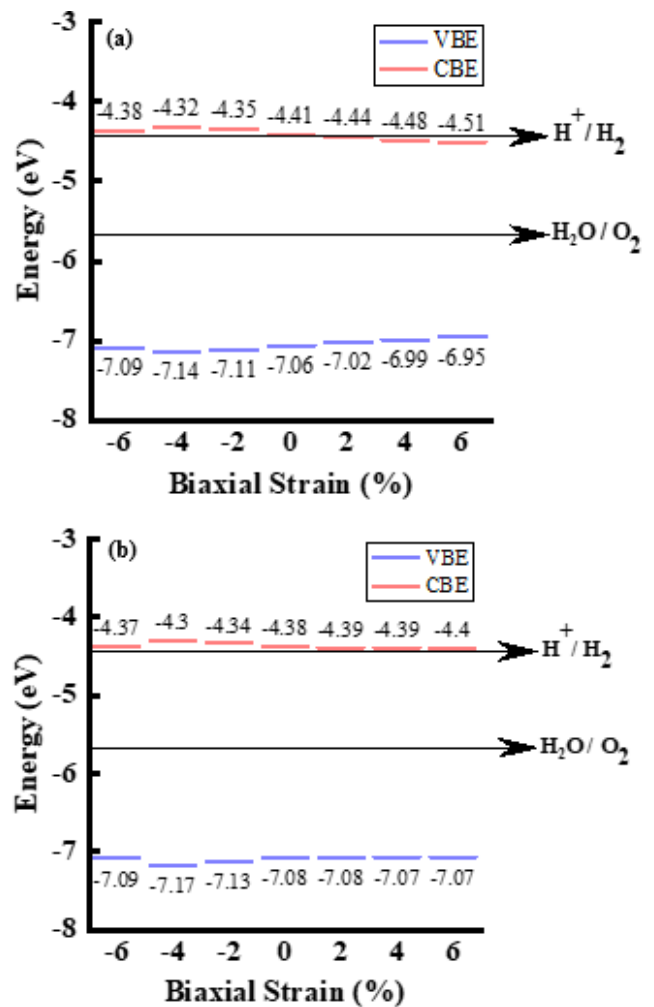


FIGURE 7. Photocatalytic overpotential (PO) with relative band positions for (a) HBL 1, and (b) HBL 6.

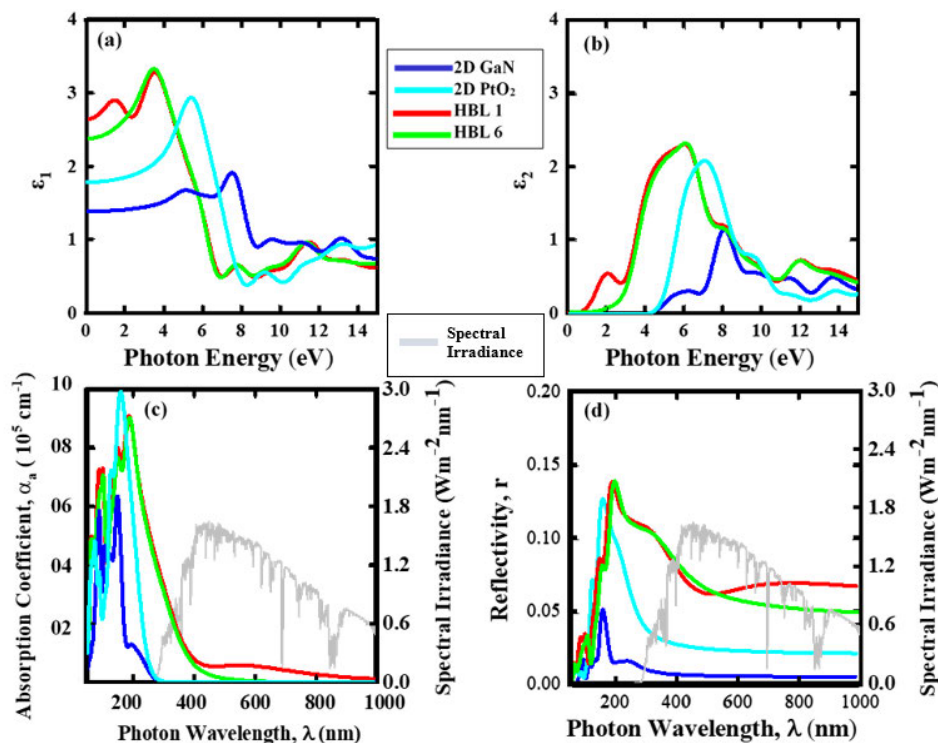


FIGURE 8. Photon energy-dependent (a) real dielectric function (b) imaginary dielectric function, and photon wavelength-dependent (c) absorption co-efficient for intrinsic, (d) reflectivity of the HBL systems.

the HBL 1 has sufficient photocatalytic overpotential (PO) up until 4% tensile strain. It has sufficient PO from 6% compressive to 4% tensile strains. The highest PO is attained at 4% compressive strain, and the overpotential for hydrogen evolution reaction (HER) is ~ 0.13 eV, and that for oxygen evolution reaction (OER) is ~ 1.47 eV. Conversely, the HBL6 has sufficient PO in all the biaxial strains either compressive or tensile in the 6% compressive to 6% tensile strains range. Again, the highest PO is achieved at 4% compressive strain and the potential for HER (OER) is ~ 0.15 eV (1.50 eV). Interestingly, 4% compressive strain the PO, facilitating the visible-light-driven PWS.

D. OPTICAL PROPERTIES AND ITS TUNABILITY UPON BIAxIAL STRAINS

Exploring optical properties and tunability of it is significant to evaluate the key performance of photocatalysts. To do so, we have calculated the core optical properties namely, real and imaginary part of the dielectric function, absorption coefficients, and reflectivity using density functional theory (DFT). The complex and imaginary part of the dielectric functions is calculated for 0 eV to 15 eV of photon energy range as demonstrated in **Fig. 8 (a), (b)**. Amazingly, no negative portion is found within the energy range in the real part of the dielectric function, revealing the semiconducting nature of the HBLs in the energy range. This property signifies the high refraction of light through the HBLs, suggesting higher photocurrent in the HBLs. The imaginary part of the

dielectric function shows the nature of the peak in the HBLs. The first peaks are also depicted in the imaginary part of the dielectric function is shown in **Fig. 8 (b)**. The first peaks are at ~ 1.8 eV, and ~ 2.01 eV for HBL 1, and HBL 6, respectively, denoting the exciton energy of the materials. Both the parts of the dielectric function follow the trend of the dielectric function of 2D PtO₂ in a red-shifted manner, suggesting a strong influence on the HBL's optical property of the substrate material. Static dielectric constant, signifying electric field supporting capability, is also calculated for the HBLs and the constituent 2D layer and the HBLs show higher value compared with the constituents. The values are as following: In HBL 1 ~ 2.74 , in HBL 6 ~ 2.5 , in 2D PtO₂ ~ 1.8 , and in 2D GaN ~ 1.45 . Clearly, a ~ 1.89 times increment of the static dielectric function value upon stacking of the layer, which indicates a significant amount of photo-induced charge supporting capability.

The optical absorption coefficient is also calculated with respect to photon wavelength which signifies the photon conversion efficacy. In our proposed HBLs, $\sim 10^6$ cm⁻¹ of absorption coefficient, 10 times greater than the perovskite materials, is attained at the ultra-violet (UV) photon wavelength, suggesting the material's high-absorption capability of photons [48], [49]. The absorption peaks again follow the trends of 2D PtO₂ in a red-shifted way. The gray lines in the **Fig. 8(c), (d)** represents solar flux (spectral irradiance), adopted in the curves for pointing out the spectrum range utilizes the most of the solar flux. It turns out that visible

TABLE 4. Benchmarking for PtO₂/GaN with 2D GaN (2D PtO₂) based VdW HBLs.

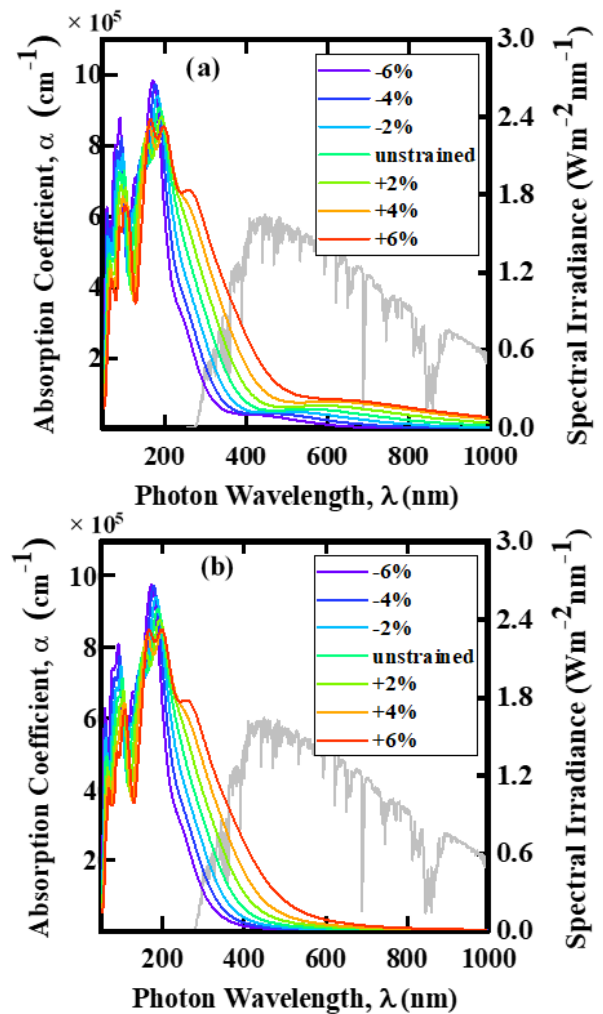
VdW HBLs	E _g (eV)	α _s (cm ⁻¹)	r (%)	PO (eV)	CBO (eV)	VBO (eV)
ZnO/GaN [35]	2.82	9×10 ⁴	-	1.2 (HER) 0.33 (OER)	0.2	0.61
GaN/GeC [15]	3.47	10 ⁵	-	0.9 (HER) 1.23 (OER)	0.06	0.97
GaN/MoSe ₂ [31]	1.7	2.1×10 ⁵	-	-	2.8	0.34
GaN/BAs [28]	1.71	3.1×10 ⁴	12	-	-	-
MoSSe/GaN [29]	1.5	3.9×10 ⁵	-	-	1.48	0.37
PtO ₂ /MoS ₂ [20]	1.5	10 ⁵	-	-	-	-
PtO₂/GaN [This work]	2.69	4.1×10⁵	7	0.15 (HER) 1.5 (OER)	1.69	2.25

PO = Photocatalytic overpotential, HER = Hydrogen evolution reaction, OER = Oxygen evolution reaction

and near infrared (NIR) hold most of the solar irradiances. The absorption coefficients and reflectivity values calculated in our work, hence compared and commented with the flux value so that the optical performance improvements of the material can be revealed.

Surprisingly, though both comprising 2D layers have zero absorption coefficient in the visible spectrum, the HBLs have $\sim 2 \times 10^5 \text{ cm}^{-1}$ (at 380 nm) of absorption coefficient, highly recommended for PWS application. To proceed further, the reflectivity of the HBLs is calculated and the highest reflectivity is $\sim 7\%$ (at 407 nm) in the visible spectrum, significantly low, suggesting the low-loss nature of the materials. These high-absorption and low-reflectivity in the visible spectrum for the HBLs suggest the visible-light-driven PWS capability of the material, as well.

To find the further visible shifting of the absorption coefficients, we have calculated the biaxial strain-dependent absorption coefficients with respect to photon wavelength. The biaxial strain tuned absorption coefficients are shown in Fig 9 (a), (b). In HBL 1, the unstrained absorption peak $\sim 9 \times 10^5 \text{ cm}^{-1}$ is at 210 nm in the UV range and in the visible range it is $2 \times 10^5 \text{ cm}^{-1}$. Upon applying compressive strains from -2% to -6% , the absorption coefficients are shifted towards the UV spectrum. Interestingly, due to the tensile strains ranges from 2% to $+6\%$, the absorption coefficient is increased by almost ~ 2 times in the visible spectrum (from 290 nm to 400 nm), significant for the PWS application. The highest absorption peak achieved in the visible spectrum for HBL 1 is $\sim 4.1 \times 10^5 \text{ cm}^{-1}$, comparable to perovskite materials. In the HBL 6, the same phenomenon is observed for the absorption co-efficient, precisely, at 6% of tensile strain, the absorption peaks in the visible region appear almost ~ 2.1 times more compared with the unstrained condition, emulating high-photocatalytic carrier generations. In the visible spectrum for HBL 6, the tensile strain tuned absorption becomes as high as $\sim 4.2 \times 10^5 \text{ cm}^{-1}$, predicting enhanced carrier generation probability of HBL 6 compared with HBL 1. Interestingly, in both HBLs, for 6% tensile strain, another absorption peak is arisen at $\sim 300 \text{ nm}$. This peak is due to the extra inter-band transition states originated

**FIGURE 9.** Biaxial strain-tuned absorption coefficient for (a) HBL 1, and (b) HBL 6. Spectral irradiance is denoted by gray line.

by the proximal transition of CBM from M^* to M and the bandgap lowering. These values also suggest that within the permissible bandgap and PO range, tensile strains in the HBL6 are more advantageous than in the HBL 1.

Concisely, the key performance factors of a photocatalysts are namely, the highest obtained bandgap, E_g , the highest optical absorption attained in the visible spectrum at a specific wavelength, α_s , reflectivity, r , photocatalytic overpotential (PO), conduction band offset (CBO), and valance band offset (VBO) are summarized in the TABLE 4 for benchmarking of this PtO₂/GaN with other 2D GaN (2D PtO₂) based vdW HBLs. These values also suggest that the PtO₂/GaN vdW HBLs can be more potential compared with their constituent layer based vdW HBLs.

IV. CONCLUSION

Harnessing first-principles density functional theory (DFT), we have explored the novel GaN/PtO₂ vdW HBL and its electronic, optical, and photocatalytic water splitting (PWS) capability. Two HBLs, HBL 1, and HBL 6 are found dynamically stable confirmed by phonon dispersion curves. Among them, the HBL 1 shows the lowest binding energy (~ 820 meV), suggesting the chemical formation feasibility of the vdW stacking. Both HBLs show visible ranged type-II bandgap. The bandgap becomes biaxial strains responsive in a manner that for both compressive and tensile strain, it tends to lower. However, some anomaly is found at 4% compressive strains due to the CBM-VBM shifting, forming the highest bandgap at this strain (~ 2.82 eV for HBL 1, and ~ 2.87 eV for HBL 6). The low-effective masses and interlayer effective potential show the spatial carrier separation probability of the HBL. Both the HBLs have sufficient photocatalytic overpotential (PO) for the HER and OER. The overpotentials are also responsive to the biaxial strains and HBL 1 has the permissible strain range is -6% to $+4\%$ while for HBL 6 it is -6% to $+6\%$. The optical absorption coefficient in the visible spectrum is $\sim 2 \times 10^5$ cm⁻¹ (at ~ 380 nm) and the value can be further improved by ~ 2 (at ~ 383 nm) times upon applying 6% tensile strain, suggesting visible-light-driven PWS capability. Concisely, the visible ranged type-II bandgap, spatial carrier separation capability, improved visible ranged absorption coefficient and tunability of the properties suggest that the novel GaN/PtO₂ VdW HBL can be a potential visible-light-driven photocatalysts candidate, fulfilling almost all the PWS attributes.

ACKNOWLEDGMENT

This work was supported by the Deanship of Scientific Research (DSR), King Abdulaziz University, Jeddah, under grant No. (DF-755-135-1441). The authors, therefore, gratefully acknowledge DSR technical and financial support.

REFERENCES

- [1] H.-T. Pao and C.-M. Tsai, "CO₂ emissions, energy consumption and economic growth in BRIC countries," *Energy Policy*, vol. 38, no. 12, pp. 7850–7860, Dec. 2010, doi: [10.1016/j.enpol.2010.08.045](https://doi.org/10.1016/j.enpol.2010.08.045).
- [2] D. Dodman, "Blaming cities for climate change? An analysis of urban greenhouse gas emissions inventories," *Environ. Urbanization*, vol. 21, no. 1, pp. 185–201, Apr. 2009, doi: [10.1177/0956247809103016](https://doi.org/10.1177/0956247809103016).
- [3] S. J. Davis and K. Caldeira, "Consumption-based accounting of CO₂ emissions," *Proc. Nat. Acad. Sci. USA*, vol. 107, no. 12, pp. 5687–5692, Mar. 2010, doi: [10.1073/pnas.0906974107](https://doi.org/10.1073/pnas.0906974107).
- [4] G. L. Chiarello, M. H. Aguirre, and E. Selli, "Hydrogen production by photocatalytic steam reforming of methanol on noble metal-modified TiO₂," *J. Catal.*, vol. 273, no. 2, pp. 182–190, Jul. 2010, doi: [10.1016/j.jcat.2010.05.012](https://doi.org/10.1016/j.jcat.2010.05.012).
- [5] T. Jafari, E. Moharrerri, A. Amin, R. Miao, W. Song, and S. Suib, "Photocatalytic water splitting—The untamed dream: A review of recent advances," *Molecules*, vol. 21, no. 7, p. 900, Jul. 2016, doi: [10.3390/molecules21070900](https://doi.org/10.3390/molecules21070900).
- [6] S. Czernik, R. Evans, and R. French, "Hydrogen from biomass—production by steam reforming of biomass pyrolysis oil," *Catal. Today*, vol. 129, nos. 3–4, pp. 265–268, Dec. 2007, doi: [10.1016/j.cattod.2006.08.071](https://doi.org/10.1016/j.cattod.2006.08.071).
- [7] J. M. Macak, M. Zlamal, J. Krysa, and P. Schmuki, "Self-organized TiO₂ nanotube layers as highly efficient photocatalysts," *Small*, vol. 3, no. 2, pp. 300–304, Feb. 2007, doi: [10.1002/sml.200600426](https://doi.org/10.1002/sml.200600426).
- [8] U. Maitra, U. Gupta, M. De, R. Datta, A. Govindaraj, and C. N. R. Rao, "Highly effective visible-light-induced H₂ generation by single-layer 1T-MoS₂ and a nanocomposite of few-layer 2H-MoS₂ with heavily nitrogenated graphene," *Angew. Chem. Int. Ed.*, vol. 52, no. 49, pp. 13057–13061, Dec. 2013, doi: [10.1002/anie.201306918](https://doi.org/10.1002/anie.201306918).
- [9] C. N. R. Rao, K. Pramoda, A. Saraswat, R. Singh, P. Vishnoi, N. Sagar, and A. Hezam, "Superlattices of covalently cross-linked 2D materials for the hydrogen evolution reaction," *APL Mater.*, vol. 8, no. 2, Feb. 2020, Art. no. 020902, doi: [10.1063/1.5135340](https://doi.org/10.1063/1.5135340).
- [10] J. Zhang, P. Zhou, J. Liu, and J. Yu, "New understanding of the difference of photocatalytic activity among anatase, rutile and brookite TiO₂," *Phys. Chem. Chem. Phys.*, vol. 16, no. 38, pp. 20382–20386, 2014, doi: [10.1039/c4cp02201g](https://doi.org/10.1039/c4cp02201g).
- [11] J. Ran, W. Guo, H. Wang, B. Zhu, J. Yu, and S.-Z. Qiao, "Metal-free 2D/2D phosphorene/g-C₃N₄ van der Waals heterojunction for highly enhanced visible-light photocatalytic H₂ production," *Adv. Mater.*, vol. 30, no. 25, pp. 2–7, 2018, doi: [10.1002/adma.201800128](https://doi.org/10.1002/adma.201800128).
- [12] A. Di Bartolomeo, "Emerging 2D materials and their van der Waals heterostructures," *Nanomaterials*, vol. 10, no. 3, pp. 1–10, Mar. 2020, doi: [10.3390/nano10030579](https://doi.org/10.3390/nano10030579).
- [13] R. Zhang, L. Zhang, Q. Zheng, P. Gao, J. Zhao, and J. Yang, "Direct Z-scheme water splitting photocatalyst based on two-dimensional van der Waals heterostructures," *J. Phys. Chem. Lett.*, vol. 9, no. 18, pp. 5419–5424, Sep. 2018, doi: [10.1021/acs.jpclett.8b02369](https://doi.org/10.1021/acs.jpclett.8b02369).
- [14] M. S. H. Khan, M. R. Islam, and M. T. Hasan, "Strain-dependent electronic and optical properties of boron-phosphide and germanium-carbide hetero-bilayer: A first-principles study," *AIP Adv.*, vol. 10, no. 8, Aug. 2020, Art. no. 085128, doi: [10.1063/5.0021359](https://doi.org/10.1063/5.0021359).
- [15] M. S. H. Khan, M. R. Islam, M. S. Islam, I. M. Mehedi, and M. T. Hasan, "Tunable photocatalytic properties of planar GaN/GeC hetero-bilayer: Production of H₂ fuel," *IEEE Access*, vol. 8, pp. 209030–209042, 2020, doi: [10.1109/ACCESS.2020.3037036](https://doi.org/10.1109/ACCESS.2020.3037036).
- [16] A. K. Singh, K. Mathew, H. L. Zhuang, and R. G. Hennig, "Computational screening of 2D materials for photocatalysis," *J. Phys. Chem. Lett.*, vol. 6, no. 6, pp. 1087–1098, Mar. 2015, doi: [10.1021/jz502646d](https://doi.org/10.1021/jz502646d).
- [17] T. Yang, T. T. Song, M. Callsen, J. Zhou, J. W. Chai, Y. P. Feng, S. J. Wang, and M. Yang, "Atomically thin 2D transition metal oxides: Structural reconstruction, interaction with substrates, and potential applications," *Adv. Mater. Interfaces*, vol. 6, no. 1, pp. 1–19, 2019, doi: [10.1002/admi.201801160](https://doi.org/10.1002/admi.201801160).
- [18] J. Zhang, Y. Xie, Y. Hu, and H. Shao, "Remarkable intrinsic ZT in the 2D PtX₂ (X = O, S, Se, Te) monolayers at room temperature," *Appl. Surf. Sci.*, vol. 532, Dec. 2020, Art. no. 147387, doi: [10.1016/j.apsusc.2020.147387](https://doi.org/10.1016/j.apsusc.2020.147387).
- [19] A. Shokri, A. Yazdani, and K. Rahimi, "Tunable electronic and optical properties of g-ZnO/ α -PtO₂ van der Waals heterostructure: A density functional theory study," *Mater. Chem. Phys.*, vol. 255, Nov. 2020, Art. no. 123617, doi: [10.1016/j.matchemphys.2020.123617](https://doi.org/10.1016/j.matchemphys.2020.123617).
- [20] J. Li and S. Y. Xie, "van der Waals PtO₂/MoS₂ heterostructure verified from first principles," *Phys. Lett. A, Gen. At. Solid State Phys.*, vol. 384, no. 14, pp. 8–11, 2020, doi: [10.1016/j.physleta.2020.126286](https://doi.org/10.1016/j.physleta.2020.126286).
- [21] L. Xie, X. Ren, Q. Liu, G. Cui, R. Ge, A. M. Asiri, X. Sun, Q. Zhang, and L. Chen, "A Ni(OH)₂-PtO₂ hybrid nanosheet array with ultralow Pt loading toward efficient and durable alkaline hydrogen evolution," *J. Mater. Chem. A*, vol. 6, no. 5, pp. 1967–1970, 2018, doi: [10.1039/c7ta09990h](https://doi.org/10.1039/c7ta09990h).
- [22] Z. Wang, Z. Liu, G. Du, A. M. Asiri, L. Wang, X. Li, H. Wang, X. Sun, L. Chen, and Q. Zhang, "Ultrafine PtO₂ nanoparticles coupled with a Co(OH)F nanowire array for enhanced hydrogen evolution," *Chem. Commun.*, vol. 54, no. 7, pp. 810–813, 2018, doi: [10.1039/c7cc08870a](https://doi.org/10.1039/c7cc08870a).

- [23] G.-Z. Wang, S.-H. Dang, W.-X. Zhao, Y.-D. Li, S.-Y. Xiao, and M.-M. Zhong, "Tunable photocatalytic properties of GaN-based two-dimensional heterostructures," *Phys. Status Solidi (B)*, vol. 255, no. 8, pp. 4–7, 2018, doi: [10.1002/pssb.201800133](https://doi.org/10.1002/pssb.201800133).
- [24] C. Sun, M. Yang, T. Wang, Y. Shao, Y. Wu, and X. Hao, "Graphene-oxide-assisted synthesis of GaN nanosheets as a new anode material for lithium-ion battery," *ACS Appl. Mater. Interfaces*, vol. 9, no. 32, pp. 26631–26636, Aug. 2017, doi: [10.1021/acsmi.7b07277](https://doi.org/10.1021/acsmi.7b07277).
- [25] Z. Y. A. Balushi, K. Wang, R. K. Ghosh, R. A. Vilá, S. M. Eichfeld, J. D. Caldwell, X. Qin, Y.-C. Lin, P. A. DeSario, G. Stone, S. Subramanian, D. F. Paul, R. M. Wallace, S. Datta, J. M. Redwing, and J. A. Robinson, "Two-dimensional gallium nitride realized via graphene encapsulation," *Nature Mater.*, vol. 15, no. 11, pp. 1166–1171, Nov. 2016, doi: [10.1038/nmat4742](https://doi.org/10.1038/nmat4742).
- [26] Q. Peng, C. Liang, W. Ji, and S. De, "Mechanical properties of g-GaN: A first principles study," *Appl. Phys. A, Solids Surf.*, vol. 113, no. 2, pp. 483–490, Nov. 2013, doi: [10.1007/s00339-013-7551-4](https://doi.org/10.1007/s00339-013-7551-4).
- [27] B. Liu, W. Yang, J. Li, X. Zhang, P. Niu, and X. Jiang, "Template approach to crystalline GaN nanosheets," *Nano Lett.*, vol. 17, no. 5, pp. 3195–3201, May 2017, doi: [10.1021/acs.nanolett.7b00754](https://doi.org/10.1021/acs.nanolett.7b00754).
- [28] A. A. Attia and H. R. Jappor, "Tunable electronic and optical properties of new two-dimensional GaN/BAs van der Waals heterostructures with the potential for photovoltaic applications," *Chem. Phys. Lett.*, vol. 728, pp. 124–131, Aug. 2019, doi: [10.1016/j.cplett.2019.05.005](https://doi.org/10.1016/j.cplett.2019.05.005).
- [29] K. Ren, S. Wang, Y. Luo, J.-P. Chou, J. Yu, W. Tang, and M. Sun, "High-efficiency photocatalyst for water splitting: A Janus MoS₂/XN (X = Ga, Al) van der Waals heterostructure," *J. Phys. D, Appl. Phys.*, vol. 53, no. 18, Apr. 2020, Art. no. 185504, doi: [10.1088/1361-6463/ab71ad](https://doi.org/10.1088/1361-6463/ab71ad).
- [30] K. Ren, Y. Luo, J. Yu, and W. Tang, "Theoretical prediction of two-dimensional ZnO/GaN van der Waals heterostructure as a photocatalyst for water splitting," *Chem. Phys.*, vol. 528, Jan. 2020, Art. no. 110539, doi: [10.1016/j.chemphys.2019.110539](https://doi.org/10.1016/j.chemphys.2019.110539).
- [31] Z. Cui, K. Ren, Y. Zhao, X. Wang, H. Shu, J. Yu, W. Tang, and M. Sun, "Electronic and optical properties of van der Waals heterostructures of g-GaN and transition metal dichalcogenides," *Appl. Surf. Sci.*, vol. 492, pp. 513–519, Oct. 2019, doi: [10.1016/j.apsusc.2019.06.207](https://doi.org/10.1016/j.apsusc.2019.06.207).
- [32] M. Sun, J.-P. Chou, J. Yu, and W. Tang, "Electronic properties of blue phosphorene/graphene and blue phosphorene/graphene-like gallium nitride heterostructures," *Phys. Chem. Chem. Phys.*, vol. 19, no. 26, pp. 17324–17330, 2017, doi: [10.1039/c7cp01852e](https://doi.org/10.1039/c7cp01852e).
- [33] K. Ren, Y. Luo, S. Wang, J.-P. Chou, J. Yu, W. Tang, and M. Sun, "A van der Waals heterostructure based on graphene-like gallium nitride and boron selenide: A high-efficiency photocatalyst for water splitting," *ACS Omega*, vol. 4, no. 26, pp. 21689–21697, Dec. 2019, doi: [10.1021/acsomega.9b02143](https://doi.org/10.1021/acsomega.9b02143).
- [34] G. Wang, W. Tang, L. Geng, Y. Li, B. Wang, J. Chang, and H. Yuan, "Rotation tunable photocatalytic properties of ZnO/GaN heterostructures," *Phys. Status Solidi (B)*, vol. 257, no. 3, pp. 1–6, 2020, doi: [10.1002/pssb.201900663](https://doi.org/10.1002/pssb.201900663).
- [35] G. Wang, L. Zhang, Y. Li, W. Zhao, A. Kuang, Y. Li, L. Xia, Y. Li, and S. Xiao, "Biaxial strain tunable photocatalytic properties of 2D ZnO/GeC heterostructure," *J. Phys. D, Appl. Phys.*, vol. 53, no. 1, 2020, Art. no. 015104, doi: [10.1088/1361-6463/ab440e](https://doi.org/10.1088/1361-6463/ab440e).
- [36] A. Mogulkoc, Y. Mogulkoc, M. Modarresi, and B. Alkan, "Electronic structure and optical properties of novel monolayer gallium nitride and boron phosphide heterobilayers," *Phys. Chem. Chem. Phys.*, vol. 20, no. 44, pp. 28124–28134, Nov. 2018, doi: [10.1039/c8cp05529g](https://doi.org/10.1039/c8cp05529g).
- [37] S. J. Clark, M. D. Segall, C. J. Pickard, P. J. Hasnip, M. I. J. Probert, K. Refson, and M. C. Payne, "First principles methods using CASTEP," *Zeitschrift für Kristallographie*, vol. 220, nos. 5–6, pp. 567–570, May 2005, doi: [10.1524/zkri.220.5.567.65075](https://doi.org/10.1524/zkri.220.5.567.65075).
- [38] J. P. Perdew, K. Burke, and M. Ernzerhof, "Generalized gradient approximation made simple," *Phys. Rev. Lett.*, vol. 77, no. 18, pp. 3865–3868, 1996, doi: [10.1103/PhysRevLett.77.3865](https://doi.org/10.1103/PhysRevLett.77.3865).
- [39] S. Grimme, "Semiempirical hybrid density functional with perturbative second-order correlation," *J. Chem. Phys.*, vol. 124, no. 3, Jan. 2006, Art. no. 034108, doi: [10.1063/1.2148954](https://doi.org/10.1063/1.2148954).
- [40] A. P. Bartók and J. R. Yates, "Regularized SCAN functional," *J. Chem. Phys.*, vol. 150, no. 16, pp. 1–6, 2019, doi: [10.1063/1.5094646](https://doi.org/10.1063/1.5094646).
- [41] S. Grimme, "Accurate description of van der Waals complexes by density functional theory including empirical corrections," *J. Comput. Chem.*, vol. 25, no. 12, pp. 1463–1473, Sep. 2004, doi: [10.1002/jcc.20078](https://doi.org/10.1002/jcc.20078).
- [42] S. H. Khan, R. Islam, and T. Hasan, "Electronic and optical properties of BeO Co-doped 2D GaN using first-principles," in *Proc. 11th Int. Conf. Electr. Comput. Eng. (ICECE)*, Dec. 2020, pp. 258–261, doi: [10.1109/ICECE51571.2020.9393143](https://doi.org/10.1109/ICECE51571.2020.9393143).
- [43] M. S. Hasan Khan, F. I. Mime, and M. R. Islam, "Electronic and optical properties of sn doped hexagonal BN monolayer: A first-principles study," in *Proc. IEEE Region 10 Symp. (TENSYP)*, Jun. 2020, pp. 230–233, doi: [10.1109/TENSYP50017.2020.9230995](https://doi.org/10.1109/TENSYP50017.2020.9230995).
- [44] Y. Yang, O. Sugino, and T. Ohno, "Band gap of β -PtO₂ from first-principles," *AIP Adv.*, vol. 2, no. 2, Jun. 2012, Art. no. 022172.
- [45] T. M. Pedersen, W. X. Li, and B. Hammer, "Structure and activity of oxidized Pt(110) and α -PtO₂," *Phys. Chem. Chem. Phys.*, vol. 8, no. 13, pp. 1566–1574, 2006, doi: [10.1039/b515166j](https://doi.org/10.1039/b515166j).
- [46] J. J. Blackstock, W. F. Stickle, C. L. Donley, D. R. Stewart, and R. S. Williams, "Internal structure of a molecular junction device: Chemical reduction of PtO₂ by Ti evaporation onto an interceding organic monolayer," *J. Phys. Chem. C*, vol. 111, no. 1, pp. 16–20, Jan. 2007, doi: [10.1021/jp066266v](https://doi.org/10.1021/jp066266v).
- [47] H. A. H. Mohammed, G. M. Dongho-Nguimdo, and D. P. Joubert, "Comprehensive first-principles study of bulk, bilayer, and monolayer α -PtO₂ properties," *Phys. E, Low-Dimension Syst. Nanostruct.*, vol. 127, Mar. 2021, Art. no. 114514, doi: [10.1016/j.physe.2020.114514](https://doi.org/10.1016/j.physe.2020.114514).
- [48] P. Tonui, S. O. Oseni, G. Sharma, Q. Yan, and G. T. Mola, "Perovskites photovoltaic solar cells: An overview of current status," *Renew. Sustain. Energy Rev.*, vol. 91, pp. 1025–1044, Aug. 2018, doi: [10.1016/j.rser.2018.04.069](https://doi.org/10.1016/j.rser.2018.04.069).
- [49] P. P. Mondal, M. R. Islam, M. S. H. Khan, and M. R. Kaysir, "Performance analysis of perovskite solar cells with different structures," in *Proc. Int. Conf. Electr., Comput. Commun. Eng.*, Feb. 2019, pp. 1–5, doi: [10.1109/ECACE.2019.8679329](https://doi.org/10.1109/ECACE.2019.8679329).



MD. SAKIB HASAN KHAN received the B.Sc.Eng. and M.Sc.Eng. degrees in electrical and electronic engineering from Khulna University of Engineering & Technology (KUET), in April 2018 and September 2020, respectively.

He has been serving as an Assistant Professor for KUET, since December 2020. He has published numerous research articles in prominent national and international conferences and journals. His core research interest includes electronic and optical properties of 2-D materials and their application in hydrogen fuel production.



MUHAMMAD SHAFFATUL ISLAM received the B.Sc.Eng. degree in electrical and electronic engineering from American International University-Bangladesh (AIUB), Dhaka, Bangladesh, in 2010, and the M.Sc.Eng. degree in electrical and electronic engineering from Khulna University of Engineering & Technology (KUET), Khulna, Bangladesh, in 2015.

He is currently working as a Lecturer with the Department of Electrical and Electronic Engineering, World University of Bangladesh (WUB), Dhaka. His current research interests include III-V-based single and double gate MOSFET, and the crystal orientation dependent characteristics of devices.



MD. RAFIQUK ISLAM (Senior Member, IEEE) received the B.Sc. degree in electrical and electronic engineering from Bangladesh University of Engineering and Technology (BUET), Bangladesh, in 1998, the M.Sc. degree in electrical and electronic engineering from Khulna University of Engineering and Technology (KUET), Bangladesh, in 2006, and the Ph.D. degree in semiconductor device growth, characterization and fabrication from University of Fukui, Japan, in 2010.

He is currently working as a Professor with KUET. He has published around 100 research articles in national and international conferences and journals. His research interests include thin films solar cells, growth characterization and fabrications, advanced semiconductor materials properties, and compound semiconductor-based devices. His two papers received the best paper award at international conferences. He received the MONBUKAGAKUSHO Scholarship from Japan (MEXT), for the period 2007–2010.

AHMED ISKANDERANI received the master's degree in electrical and computer engineering from the University of California, USA, and the Ph.D. degree in computer information and control engineering from the University of Michigan, Ann Arbor, USA, in 1984.

He was the Director of the Computer Center at King Abdulaziz University (KAU), Jeddah, Saudi Arabia, where he led several strategic information systems, such as student's registration and record systems, HR and finance systems, and library automation. He worked at the Islamic Development Bank (IsDB), an international financial institution, for many years, where he held a couple of the director level positions. Lately, he was the Acting Director General of The Islamic Research and Training Institute (IRTI) and a member of IsDB Group. He is currently an Associate Professor of electrical and computer engineering (ECE) with KAU. He taught a huge number of courses at KAU ECE, including a full master's program in Internet protocols and software engineering. He has supervised many B.Sc. graduation projects and a number of master's degree thesis in the areas of computer engineering, software engineering, and optimization. He founded a massive open online course (MOOC) program with edX an establishment by Harvard and MIT universities. Several MOOCs in Islamic economics and finance has been offered globally in this program, where thousands of students attended.

Dr. Iskanderani is a member of the Board of Directors for the Arab Fund for Scientific Research. He was the Secretary of the Board of Trustees, IRTI, and the Vice Chairman of the Board of Trustees, Virtual Islamic University, a project established by the Federation of the Universities of the Islamic World.

IBRAHIM M. MEHEDI (Member, IEEE) received the B.Sc. degree (Hons.) in electrical and electronic engineering from Rajshahi University of Engineering and Technology (RUET), Bangladesh, in 2000, the M.Sc. degree in aerospace engineering from University Putra Malaysia (UPM), Malaysia, in 2005, and the Ph.D. degree in electrical engineering and information systems from The University of Tokyo, Tokyo, Japan, in 2011. After his B.Sc. degree, he worked at Coca-Cola Bottling Plant, for two years. He was appointed as a Lecturer with the King Fahd University of Petroleum and Minerals (KFUPM), in 2006. He worked as a Research Assistant and a Postdoctoral Fellow with Japan Aerospace Exploration Agency (JAXA), Japan, from 2008 to 2012. He joined the Department of Electrical and Computer Engineering (ECE), King Abdulaziz University (KAU), in 2012, where he is currently an Associate Professor. He is also a Senior Scientist of the Center of Excellence in Intelligent Engineering Systems (CEIES), King Abdulaziz University. He was the Principal Investigator in large research and development projects funded by KACST, MOE, and KAU. He has been involved in several research and development projects. He has published several journals and conference papers, and supervised and co-supervised several M.Sc. and Ph.D. students. His field of interests and specializations covers a broad spectrum from theoretical to practical aspects of engineering, including intelligent systems, control, electronic devices, sensors, energy, and artificial intelligence.



MD. TANVIR HASAN (Senior Member, IEEE) received the B.Sc. and M.Sc. degrees in electrical and electronic engineering from Khulna University of Engineering & Technology (KUET), Bangladesh, in 2006 and 2007, respectively, and the Ph.D. degree in electrical and electronic engineering from the Graduate School of Engineering, University of Fukui, Japan, in 2013.

He is currently working as an Associate Professor with the Department of Electrical and Electronic Engineering, Jashore University of Science and Technology (JUST), Bangladesh. He has authored or coauthored more than 50 research papers in conferences and journals. His research interest includes growth, design, fabrication, characterization, simulation, and modelling of III-V-based semiconductor devices (electronic and optoelectronic). He has been a member of the IEEE Electron Devices Society, since 2008. He served as the Secretary for the IEEE Young Professional, Bangladesh Section (BDS), and an Executive Committee Member and a Professional Activity Coordinator for the IEEE BDS, in 2016 and 2017, respectively. He received the IEEE Student Paper Award (Honorary Mentioned), from the IEEE Electron Devices Society, Bangladesh Chapter, in 2007. He received the MONBUKAGAKUSHO Scholarship from Japan (MEXT), for the period 2010–2013. He serves as a Reviewer for IEEE TRANSACTIONS ON ELECTRON DEVICES, *Journal of Applied Physics*, and *Applied Physics Letters*.

...